Analytical model for the optimal design of a brushless DC wheel motor

S. Brisset and P. Brochet

L2EP, Ecole Centrale de Lille, Cité Scientifique, Villeneuve d'Ascq, France

Abstract

Purpose – Analytical models are often used in the first steps of the design process. They are associated with optimisation methods to find a solution that fulfil the design specifications. In this paper, the analytical model of an electric motor is built and proposed as a benchmark to highlight the optimisation methods the most fitted to analytical models.

Design/methodology/approach – This paper studies the optimal design of a brushless DC wheel motor. First, the analytical model is presented. Each equation used for the sizing is described, including the physical phenomenon associated, the hypotheses done, and some precautions to take before computing. All equations are ordered to ease their resolution, due to a specific procedure which is then described. Secondly, three optimisation problems with an increasing number of parameters and constraints are proposed. Finally, the results found by the sequential quadratic method point out the special features of this benchmark.

Findings – The constraint optimisation problem proposed is clearly multimodal as shown in the results of one deterministic method. Many starting points were used to initialise the optimisation methods and lead to two very different solutions.

Originality/value – First, an analytical model for the optimal design is detailed and each equation is explained. A specific procedure is presented to order all equations in order to ease their resolution. Secondly, a multimodal benchmark is proposed to promote the development of hybrid methods and special heuristics.

Keywords Optimization techniques, Design, Electric motors

Paper type Research paper

1. Introduction

The optimal design of electromagnetic structures using global optimisation techniques is a field of research with a wide range of applications. Actually many international conferences are devoted entirely (OIPE) or include topics on the optimisation of electromagnetic devices (COMPUMAG, CEFC, EMF, ISEF, . . .).

COMPUMAG Team workshop proposes two benchmarks on optimisation that are a superconducting magnetic energy storage (SMES) device (www.igte.tu-graz.ac.at/archive/team/index.htm) and a die press model (http://ics.ec-lyon.fr/problems/problem25.pdf). Both use a finite element model to compute the objective function and the constraints. Due to them, the optimisation methods that are most fitted to this kind of optimisation are pointed out.

Finite element analyses (FEA) are essential for the design of electromagnetic devices, but they are not the only ones. Analytical models are often used in the first steps of the design process where decisions on the structure of the device and the materials used have to be taken. Indeed, they have some advantages over FEA: they are faster and can be used with a higher number of parameters; they are more flexible

and take into account the physical phenomena of different natures. Moreover, the analytical models can be set up in order to manage the design problem by solving the inverse problem, i.e. find the geometrical dimensions of the device directly from the knowledge of the specifications. On the contrary, FEA can just compute the specifications when the geometrical dimensions are known and require iterative optimisation techniques to solve the design problem. The main drawbacks of analytical models are the lower accuracy in each physic domain and the amount of knowledge required for their development.

Few analytical models exist that are able to be proposed as benchmarks for optimisation methods (Fitan et al., 2004; Higuchi et al., 2002). Indeed, the models are rarely sufficiently detailed or associated to a well-formalised specification sheet. This paper presents the sizing model of an original motor that on the one hand is complete and can be used as a benchmark for optimisation methods. On the other hand, it is explained sufficiently and detailed to be adapted to different design contexts.

This paper studies the optimal design of a brushless DC wheel motor. First, the analytical model is presented. Each equation used for the sizing is described, including the physical phenomenon associated, the hypotheses done, and some precautions to take before computing. All equations are ordered to ease their resolution, due to a specific procedure which is then described. Secondly, three optimisation problems with an increasing number of parameters and constraints are proposed. Finally, the results found by the sequential quadratic method programmed in Pro@Design (www.designprocessing.com) point out the special features of this benchmark, notably its multimodality. It can be used thus to build-up hybrid optimisation methods or some search heuristics.

2. Pre-sizing model
2.1 Structural and technological choices
The motor that has to be designed is a wheel motor which propels a solar vehicle during a race. The structural and technological choices depend on this situation. Indeed, the materials and the manufacturing costs are not essential while the motor efficiency and the axial bulk are the key points.

Therefore, a brushless DC motor with surface SmCo magnets, concentrated windings, radial flux, and outer rotor (Miller and Hendershot, 1994) is preferred as explained in Brisset et al. (2001). An inverter with hysteresis regulated current drives the motor by using the information of three Hall sensors.

2.2 Equations for sizing
Generally, it is easier to start from the geometrical dimensions of a device and to deduce its specifications, such as efficiency and temperature. This is called a direct model and requires iterative optimisation techniques to be reversed, i.e. leads to geometrical dimensions when the specifications of the device are known. The non-iterative computation of the geometrical dimensions can be made by using some hypotheses that lead to an inverse model which is simpler and suitable for the pre-sizing of the device.

The constitutive analytical equations are non-linear and describe physical phenomena in various fields, e.g. thermal, mechanical, magnetic, and electrical. Their origin is described as well as possible precaution when using them.

2.2.1 Electromechanical conversion. The expression of the electromagnetic torque C can be obtained from the electromagnetic power given in equation (1):

$$P_{em}(t) = C(t)\Omega(t) = \sum_{i=1}^{m} e_i(t)i_i(t) \qquad (1)$$

where Ω is the rotation speed, m the number of phases, e_i is the electromotive force (EMF) of phase i, and i_i is the current in phase i. In the case of a brushless DC with three phases and square-wave currents, the EMF is equal to $+E$ during 120 electrical degrees, zero or an indeterminate value during 60 electrical degrees, $-E$ during 120 electrical degrees, and zero or an indeterminate value during 60 electrical degrees. For a wye connection, two phases are on simultaneously and the waveform of the current is as shown in Figure 1 with a peak value equal to $+I$. Therefore, at constant speed, the electromagnetic power is constant and equation (1) becomes:

$$C\Omega = 2EI \qquad (2)$$

2.2.2 Lenz's law. The EMF is computed from the variation of the flux linkage of one coil by using the Lenz's law. When the rotor's displacement is equal to the pole
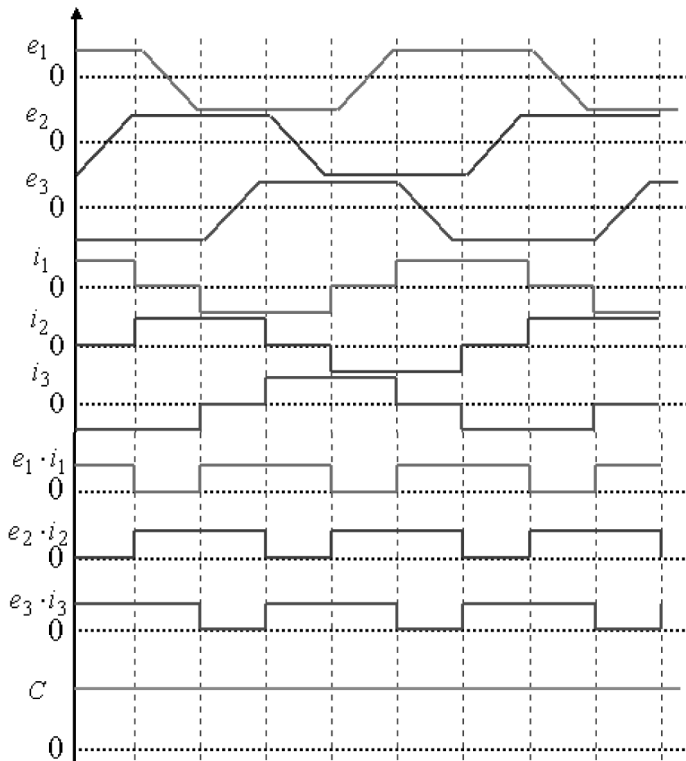

Figure 1.
EMFs, currents, electromagnetic powers for the three phases, and electromagnetic torque resulting. A vertical line is placed all 60 electrical degrees

pitch, i.e. π/p, a south magnet takes the place of a north magnet and the flux ϕ reverses, thus:

$$E = \frac{n}{4}\frac{\mathrm{d}\phi}{\mathrm{d}\theta}\frac{\mathrm{d}\theta}{\mathrm{d}t} = \frac{n}{4}\frac{2\phi}{\pi/p}\Omega \tag{3}$$

where n is the number of supplied conductors, i.e. the two-third of the total number of conductors, and the number of magnets is $2p$. The flux ϕ is given when a north magnet is just in front of the coil:

$$\phi = B_e S_p \tag{4}$$

where S_p is the surface of a magnetic pole, and B_e is the maximum magnetic induction in the air gap. Equation (3) is built from the hypothesis of a by parts linear variation of the flux versus the rotor position. This gives to a constant by parts EMF. By combining equations (2)-(4), the electromagnetic torque expression becomes:

$$C = nIB_e\frac{S_e}{2\pi} \tag{5}$$

$$S_e = 2pS_p \tag{6}$$

where S_e is the total area of the air gap. Equation (5) shows that the electromagnetic torque produced by a brushless DC motor (BLDC) is proportional to the air gap area multiplied by the magnetic induction in the air gap and nI, i.e. the magnetomotive force (MMF) created by the coils.

For a radial flux BLDC motor, the total air gap area is:

$$S_e = \pi D_s L_m \tag{7}$$

where D_s is the bore (stator) diameter and L_m is the magnetic length of the motor, i.e. the length of the stack of metal sheets. Equations (3), (4), (6) and (7) lead to:

$$E = \frac{n}{4}B_e D_s L_m \Omega \tag{8}$$

A more general approach can be used to give the expression of the EMF. Figure 2 shows a simplified view of the magnetic parts in the vicinity of the air gap. Their characteristics condition the EMF waveform. With the hypotheses of a constant air gap thickness and
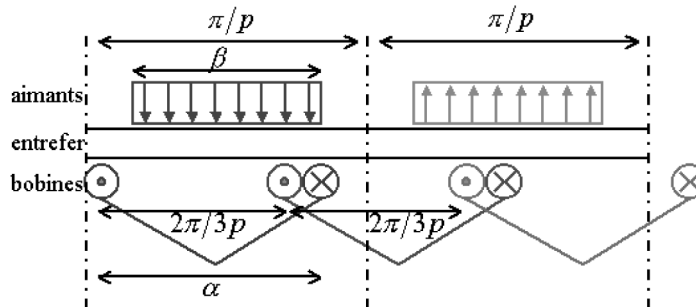

Figure 2.
Vicinity of the air gap, magnets and coils of the stator

purely radial magnetic induction in the air gap and magnets, the waveform of the magnetic induction in the air gap is as shown in Figure 3. The flux across the coil is computed by integration of the magnetic induction on the area enclosed by the coil borders, defined by the angle α in the cross section. Similarly, the EMF is calculated by derivation of the flux across the coil, giving then the waveforms shown in Figure 4. Let us note that the expression of the EMF is unchanged, but it is now possible to fix the width of the magnets and the opening of the coils so that the flux is maximum, in accordance with equation (4), and that the plateau of EMF is the largest possible:

$$\alpha = \frac{\pi}{p} \qquad (9)$$

$$\beta = \frac{\pi}{p} \qquad (10)$$

FEA have been requested to refine this first analytic approach (Brisset *et al.*, 2000). An analysis of sensitivity of the width of the plateau of EMF indicated the same tendencies as that of the analytic approach. However, the variation is non-linear for the parameters α and β. Besides, it has been shown that an intermediate tooth in the middle of every slot was necessary to get a trapezoidal EMF and that the width of its widening α_i has a strong influence. The following relation has been established for a structure with a ratio
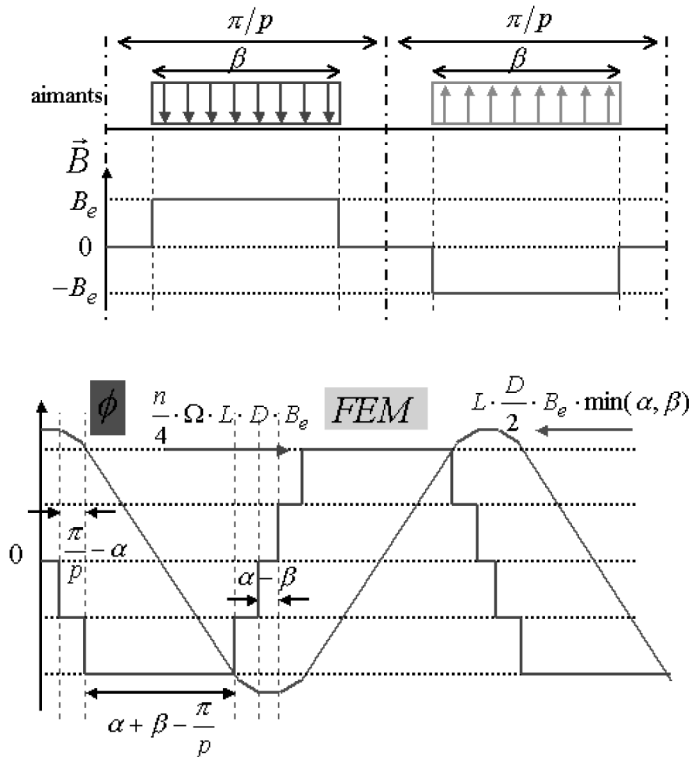

Figure 3.
Magnetic induction
waveform in the air gap

Figure 4.
Flux and EMF waveforms

of the number of slots on the number of magnets equal to 3/4 and assuming that the stator is sufficiently smooth so that the distribution of the induction in the air gap is in conformity with the hypotheses but not too much to avoid to create a magnetic shunt between coils.

$$\alpha_i = \frac{\alpha}{5} \tag{11}$$

2.2.3 Geometrical relations. The main geometric parameters are shown in Figure 5. The distances are noted in Latin alphabet and the angles are noted in Greek alphabet. These parameters permit to write several relations of geometric nature:

$$S_{enc} \approx hd\left[2\pi\left(\frac{D_s}{2} - eb\right) - \pi hd - N_e(li + ld)\right] \tag{12}$$

$$S_{enc}k_r = \frac{3}{2}n\frac{I}{\delta} \tag{13}$$

$$D_{ext} = D_s + 2(e + ha + hcr) \tag{14}$$

$$D_{int} = D_s - 2(eb + hd + hcs) \tag{15}$$

$$hc = \frac{eb}{\cos(\alpha/2)} - \frac{D_s}{2}\left(\frac{1}{\cos(\alpha/2)} - 1\right) \tag{16}$$

$$hi = \frac{D_s}{2}\left[1 - \cos\left(\frac{\alpha_i}{2}\right)\right] + hc\cos\left(\frac{\alpha_i}{2}\right) \tag{17}$$

where S_{enc} is the total section of the slots, $k_r < 1$ the slot filling factor, δ the current density in the conductors, D_{ext} and D_{int} are the outer and inner diameters, respectively,
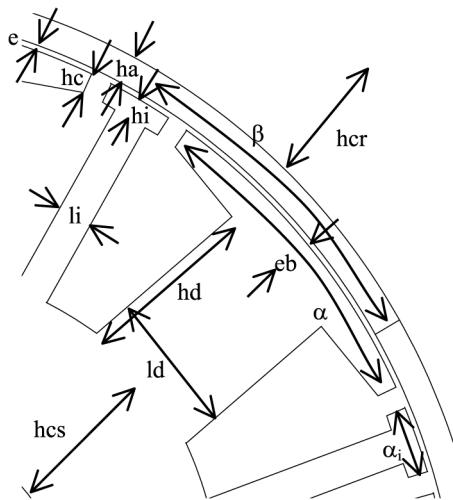

Figure 5.
Geometric parameters of the BLDC motor with radial flux, concentrated winding, permanent magnets and outer rotor

and N_e is the number of slots. The height of hold hc is calculated to get a right angle between the main tooth and the pole shoe. The central thickness of the widening of the intermediate tooth hi is calculated so that the height to the extremity of an intermediate tooth is the same as the one of a main tooth, i.e. hc, and that there is a right angle between the intermediate tooth and its shoe.

The means radius of a coil end can be approached by:

$$R_{tb} \approx \frac{ld - li}{4} + \left(\frac{D_s}{2} - eb - \frac{hd}{2}\right)\frac{\pi}{2N_e} \tag{18}$$

The medium length of a half turn is therefore:

$$L_{ds} \approx \frac{L_m}{k_{foi}} + \pi R_{tb} \tag{19}$$

where $k_{foi} < 1$ is the bulk factor of the metal sheets.

It is also possible to calculate the total axial length of the motor L_{tot} as well as the masses of the different active parts:

$$L_{tot} \approx \frac{L_m}{k_{foi}} + 2\left[\left(\frac{D_s}{2} - eb - \frac{hd}{2}\right)\frac{\pi}{N_e} - \frac{li}{2}\right] \tag{20}$$

$$M_a = d_a p \beta ha\left[ha + 2\left(\frac{D_s}{2} + e\right)\right]L_m r_{rs} \tag{21}$$

$$M_{cr} = d_{cr}\pi hcr\left[hcr + 2\left(\frac{D_s}{2} + e + ha\right)\right]L_m r_{rs} \tag{22}$$

$$M_{cs} = d_t \pi hcs\left[2\left(\frac{D_s}{2} - eb - hd\right) - hcs\right]L_m \tag{23}$$

$$M_{ds} \approx d_t N_e\left[(ld + li)hd + \left(\alpha\frac{eb + hc}{2} + \alpha_i\frac{hi + hc}{2}\right)\frac{D_s}{2}\right]L_m \tag{24}$$

$$M_{cu} = d_{cu}\frac{3}{2}n\frac{I}{\delta}L_{ds} \tag{25}$$

$$M_{tot} = M_a + M_{cr} + M_{cs} + M_{ds} + M_{cu} \tag{26}$$

where M_a, M_{cr}, M_{cs}, M_{ds}, M_{cu}, d_a, d_{cr}, d_t, and d_{cu} are the mass and the density of the magnets, the rotor yoke, the stator yoke, the teeth of the stator and the copper, respectively. M_{tot} is the total mass of the active parts and $1.2 \geq r_{rs} \geq 1/k_{foi}$ is the ratio of the length of the rotor on one of the stator.

2.2.4 Flux conservation. The average magnetic induction in the teeth is B_d, B_a in the magnets, B_{cr} in the rotor yoke, and B_{cs} in the stator back iron. Plate 1 and Figure 6 help towards the understanding of the following equations. The conservation of the flux

836

Component: BMOD
8.23127E-07   1.039513   2.079026
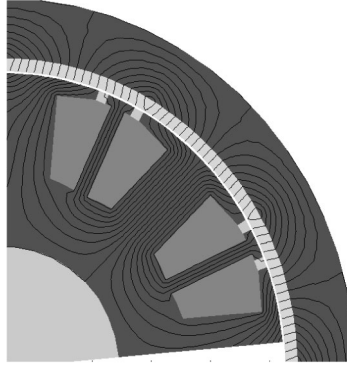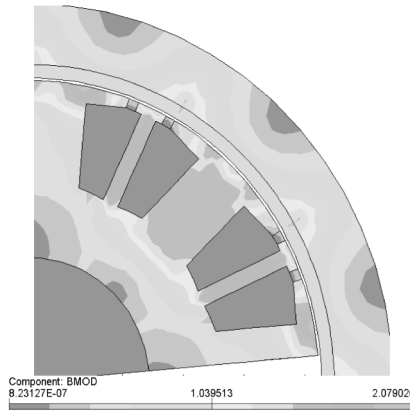
between a main tooth and its widening, named pole shoe, gives:

$$B_d l d = B_e \alpha \frac{D_s}{2} \tag{27}$$

The same relation applies between an intermediate tooth and its widening:

$$B_d l i = B_e \alpha_i \frac{D_s}{2} \tag{28}$$

The thickness of the pole shoe is calculated to permit the passage of the flux received by the part of the pole shoe passing the main tooth, so, the flux conservation gives:

$$B_d \left[eb - \frac{D_s}{2} \left(1 - \cos \left(\sin^{-1} \left(\frac{ld}{D_s} \right) \right) \right) \right] = B_e \left[\frac{\alpha}{2} - \sin^{-1} \left(\frac{ld}{D_s} \right) \right] \frac{D_s}{2} \tag{29}$$

Half of flux crossing the magnet leaves one side of the rotor yoke whereas other half leaves the other side, thus the conservation of flux between the magnet and the rotor yoke gives:

$$\frac{1}{2}B_a\beta\left(\frac{D_s}{2}+e\right) = B_{cr}hcr \tag{30}$$

Similarly, the conservation of flux between the main teeth and the stator yoke leads to:

$$\frac{1}{2}B_d ld = B_{cs}hcs \tag{31}$$

Finally, the conservation of the flux between a magnet and a main tooth in conjunction gives:

$$\left[B_a\beta\left(\frac{D_s}{2}+e\right)r_{rs}\right]k_{fui} = B_e\alpha\frac{D_s}{2} \tag{32}$$

where $k_{fui} < 1$ is a leakage coefficient, determined by finite element simulations, that express the fact that the leakage flux between the magnets cross the rotor and a part of the air gap but does not reach the stator.

2.2.5 Ampere's law. It provides a relation between the geometric parameters of the magnets, those of the magnetic circuit, the MMF created by the coils and the magnetic inductions in the different parts.

At no-load, Ampere's law gives:

$$\frac{B_{cr}}{\mu_{cr}(B_{cr})}\left[\frac{hcr}{2}+\frac{\pi}{2p}\left(\frac{D_s}{2}+e+ha+\frac{hcr}{2}\right)\right]$$
$$+\left(\frac{B_a-B_r(1+\alpha_a T_a)}{\mu_a}\right)ha+B_e e+\frac{B_d}{\mu_t(B_d)}(eb+hd) \tag{33}$$
$$+\frac{B_{cs}}{\mu_t(B_{cs})}\left[\frac{hcs}{2}+\frac{\pi}{N_e}\left(\frac{D_s}{2}-eb-hd-\frac{hcs}{2}\right)\right]=0$$

where μ_{cr} and μ_t are the relative magnetic permeabilities of the rotor yoke and sheet metal that depend on the induction level. μ_a, B_r, $\alpha_a < 0$ and T_a are, respectively, the relative permeability, the remnant induction of the magnets to 0°C, its thermal coefficient and the temperature of the magnets.

While supposing that the magnetic permeabilities of the sheet metal and the rotor yoke are more than 1,000 times superior to the one of the vacuum and therefore that the MMF consumed in the magnetic circuit is negligible in relation to those consumed in the air gap, equation (33) simplifies itself by:

$$\left(\frac{B_a-B_r(1+\alpha_a T_a)}{\mu_a}\right)ha+B_e e=0 \tag{34}$$

When the motor is in charge, some current circulates in the coils. For an abnormally high current, the magnetic induction in the magnets can reach a critical value provoking a demagnetisation. The induction being then weak, the magnetic permeability is high and it is justified to disregard the MMF consumed in the magnetic circuit. For a critical

magnetic induction in the magnets B_c, the phase current takes its admissible peak value and Ampere's law becomes, while exploiting equation (32):

$$\left(\frac{B_c - B_r(1 + \alpha_a T_a)}{\mu_o \mu_a}\right)ha + \frac{nI_{max}}{4p} \quad + \frac{B_c}{\mu_o}\frac{\beta}{\alpha}\left(1 + \frac{2e}{D_s}\right)r_{rs}k_{fui}e = 0 \tag{35}$$

2.2.6 Calculation of losses. The resistance of a phase is:

$$R_{ph} = \rho_{cu}(1 + \alpha_{cu} T_{cu})\frac{n}{2}L_{ds}\frac{\delta}{I} \tag{36}$$

where ρ_{cu} is the resistivity of the copper to 0°C, $\alpha_{cu} > 0$ is its thermal coefficient, and T_{cu} is the temperature of the coils. The copper losses are therefore:

$$P_j = 2R_{ph}I^2 \tag{37}$$

The frequency of the fundamental is:

$$f = \frac{p\Omega}{2\pi} \tag{38}$$

The iron losses are:

$$P_f = q_t \left(\frac{f}{f_t}\right)^{1.5}\left[M_{cs}\left(\frac{B_{cs}}{B_t}\right)^2 + M_{ds}\left(\frac{B_d}{B_t}\right)^2\right] \tag{39}$$

where q_t represents the specific loss for a frequency f_t and an induction B_t. The efficiency is:

$$\eta = \frac{C\Omega - P_m}{C\Omega + P_j + P_f} \tag{40}$$

where P_m are the mechanical losses.

2.2.7 Thermal model. The thermal model is very simple. On the one hand, it is supposed that the thermal resistances of conduction are always very lower than the thermal resistances of convection. Thus, the temperature is the same in all pieces of the stator in contact, which are the coils, the teeth and the stator yoke.

On the other hand, even though the stator and the rotor are not in contact by the rolling; big surfaces are face-to-face with a space of air of the order of the tenth of millimetre. In these conditions, the captive air is modelled like a material of weak thermal conductivity. In spite of it, the thermal resistance between the rotor and the stator is weak since it is equal to the thickness of air divided by the thermal conductivity and the surfaces that are face-to-face. Thus, the gradient of temperature inside the motor is weak and it is supposed that all active materials have the same temperature:

$$T_a = T_{cu} \tag{41}$$

In the hypothesis of a closed motor, the outside surface of the motor on which occurs the convection is:

$$S_{\text{ext}} = \frac{\pi}{2} D_{\text{ext}}^2 + \pi D_{\text{ext}} L_{\text{tot}} \tag{42}$$

The temperature of the motor is therefore:

$$T_{\text{cu}} = T_{\text{ext}} + \frac{P_{\text{j}} + P_{\text{f}} + P_{\text{m}}}{h S_{\text{ext}}} \tag{43}$$

where h is the coefficient of convection in air and T_{ext} is the temperature of the ambient air.

2.2.8 Converter. The knowledge of the inductance of the motor is essential to the survey of the commutations in the phases. Its value is calculated, during a steady rotor simulation, while replacing the magnets by air and while supplying two phases in series (Plate 2). The inductance of phase is given by:

$$L_{\text{ph}} I_{\text{rc}} = \psi_{\text{rc}} \tag{44}$$

where I_{rc} is the current during this steady rotor trial and ψ_{rc} is the total flux, seen by the phase, produced by this current. It decomposes in a radial flux that crosses the air gap ψ_{ent} and tangent fluxes in the slots ψ_{enc} and in the pole shoe ψ_{bec} (Plate 2):

$$\psi_{\text{rc}} = \frac{3}{2} \psi_{\text{ent}} + 2(\psi_{\text{enc}} + \psi_{\text{bec}}) \tag{45}$$

The coefficient 3/2 permits to take into account the mutual fluxes with the other phases whereas the coefficient 2 indicates that the slots and pole shoes surrounding the tooth are crossed by the same leakage flux.

By using Ampere's law, it can be found that the magnetic induction in a rectangular slot is expressed with:

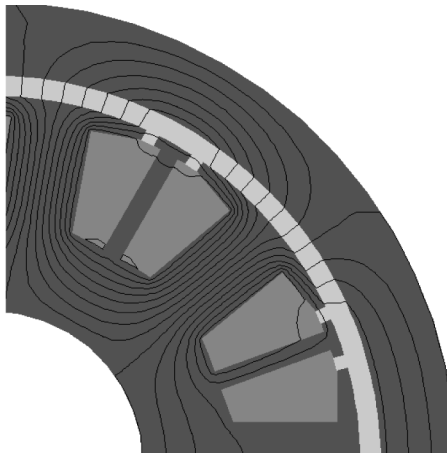$$B_{\text{enc}}(x) = \mu_o \frac{n_{\text{enc}} \cdot I_{\text{rc}}}{l_{\text{enc}}} \frac{x}{h_{\text{enc}}} \tag{46}$$

Plate 2.
Flux during a steady rotor
FEA, magnets removed

where l_{enc} is the width of the slot, h_{enc} the height of the slot, n_{enc} the number of conductors in the slots, and x the distance from the bottom of the slot, at the opposite of the air gap. Therefore, the flux crossing a rectangular slot is:

$$\psi_{\text{enc}} = \mu_o \frac{n_{\text{enc}}^2 \cdot I_{\text{rc}}}{l_{\text{enc}}} \frac{L_{\text{m}} h_{\text{enc}}}{3} \tag{47}$$

Using the parameters of the motor, the flux per current unit expresses as:

$$\frac{\psi_{\text{enc}}}{I_{\text{rc}}} = \mu_o \frac{1}{16} \frac{n^2}{N_{\text{e}}} \frac{L_{\text{m}} \cdot hd}{\left(\frac{D_{\text{s}}}{2} - eb - \frac{hd}{2}\right)\frac{\pi}{N_{\text{e}}} - \frac{ld+li}{2}} \tag{48}$$

Ampere's law gives the flux per current unit across the air gap and the pole shoe:

$$\frac{\psi_{\text{ent}}}{I_{\text{rc}}} = \mu_o \frac{3}{16} \frac{n^2}{N_{\text{e}}} \frac{L_{\text{m}}}{e + ha} \alpha \frac{D_{\text{s}}}{2} \tag{49}$$

$$\frac{\phi_{\text{bec}}}{I_{\text{rc}}} = \mu_o \frac{3}{16} \frac{n^2}{N_{\text{e}}} \frac{L_{\text{m}} hc}{\left(\frac{D_{\text{s}}}{2} - \frac{hc}{2}\right)\left(\frac{\pi}{N_{\text{e}}} - \frac{\alpha+\alpha_i}{2}\right)} \tag{50}$$

Equations (44) and (45) give:

$$L_{\text{ph}} = \frac{3}{2} \frac{\psi_{\text{ent}}}{I_{\text{rc}}} + 2\left(\frac{\psi_{\text{enc}}}{I_{\text{rc}}} + \frac{\psi_{\text{bec}}}{I_{\text{rc}}}\right) \tag{51}$$

Only the relations (48)-(51) will be used during the sizing for the calculation of the inductance in which the current I_{rc} disappears.

The converter's role is to supply the phases of the motor as shown in Figure 1. All 60 electric degrees, a commutation occurs. In the one drawn in Figures 7-9, the current of the phase 3 goes from $+I$ to 0 whereas one of the phase 1 goes from 0 to $+I$ and the one of the phase 2 maintains itself to $-I$.

Kirchhoff's laws (Figure 9) give:

$$U_{\text{DC}} = R_{\text{ph}} i_1 + L_{\text{ph}} \frac{di_1}{dt} + e_1 - R_{\text{ph}} i_2 - L_{\text{ph}} \frac{di_2}{dt} + e_2 \tag{52}$$

$$0 = R_{\text{ph}} i_2 + L_{\text{ph}} \frac{di_2}{dt} + e_2 - R_{\text{ph}} i_3 - L_{\text{ph}} \frac{di_3}{dt} + e_3 \tag{53}$$
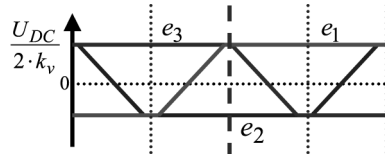
$$i_1 + i_2 + i_3 = 0 \tag{54}$$

Figure 7.
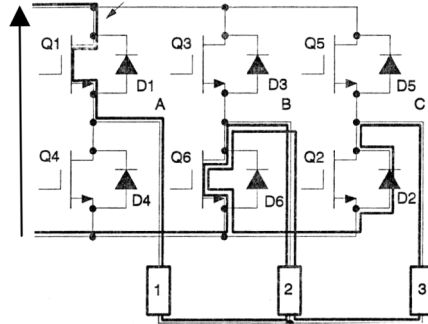State of the EMFs during
the commutation

Figure 8.
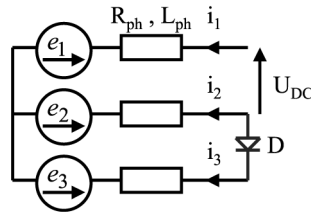Currents in the phases
during the commutation

Figure 9.
Simplified circuit during
the commutation

where U_{DC} is the voltage of the DC bus. The EMFs during the commutation (in the middle of Figure 7) are:

$$e_1 = e_3 = -e_2 = \frac{U_{DC}}{2k_v} = E \tag{55}$$

where $k_v > 1$ is the ratio between the half of the voltage of the DC bus and the EMF at the rated speed. Thus, the current in phase 1 is governed by the following differential equation:

$$R_{ph}i_1 + L_{ph}\frac{di_1}{dt} = \frac{U_{DC}}{3}\left(2 - \frac{1}{k_v}\right) \tag{56}$$

Its expression is therefore:

$$i_1(t) = \frac{U_{DC}}{3R_{ph}}\left(2 - \frac{1}{k_v}\right)\left[1 - \exp\left(-\frac{R_{ph}}{L_{ph}}t\right)\right] \tag{57}$$

The current reaches its peak value to the time:

$$t_1 = -\frac{L_{ph}}{R_{ph}}\ln\left[1 - \frac{3R_{ph}I}{U_{DC}(2 - 1/k_v)}\right] \tag{58}$$

Similarly, the expression of the current in phase 3 is:

$$i_3(t) = I\exp\left(-\frac{R_{ph}}{L_{ph}}t\right) - \frac{U_{DC}}{3R_{ph}}\left(1 + \frac{1}{k_v}\right)\left[1 - \exp\left(-\frac{R_{ph}}{L_{ph}}t\right)\right] \tag{59}$$

It appears that the current in phase 3 decreases with a slop different from that of the growth of the current in the phase 1. Thus, according to the speed of the motor and the coefficient k_v, the current in phase 2 will not be constant and will present a hollow or a peak. FEA shows this phenomenon for the rated speed and $k_v = 1.67$ (Figures 10 and 11). The hollows of current in the phase that is not in commutation are visible all 60 electrical degrees (ten mechanical degrees) and accompany torque hollow. The presented torque is calculated with Maxwell's tensor, so the reluctant torque is also visible. In the sizing process only equations (55) and (58) will be used to verify that the rise time of the current is reasonable.

The coefficient k_v has a direct influence on the maximal speed of the motor at no-load Ω_{max}:

$$\Omega_{max} = \Omega \frac{U_{DC}}{2E} \tag{60}$$

With equation (55), equation (60) becomes:

$$\Omega_{max} = k_v \Omega \tag{61}$$

Only equations (55), (58), and (61) are used in the sizing program.

2.2.9 Material properties. The known material properties are: $k_r = 0.5$, $B_r = 1.045\,\text{T}$, $B_c = 0.05\,\text{T}$, $\alpha_a = -5 \times 10^{-4}/\text{K}$, $\mu_a = 1.05$, $\mu_o = 4\pi \times 10^{-7}\,\text{T m/A}$, $\rho_{cu} = 1.72 \times 10^{-8}\,\Omega\text{m}$, $\alpha_{cu} = 3.8 \times 10^{-3}/\text{K}$, $d_t = 7{,}850\,\text{kg/m}^3$, $d_a = 7{,}400\,\text{kg/m}^3$, $d_{cu} = 8{,}950\,\text{kg/m}^3$,

Figure 10.
Currents in the three phases at full load. The horizontal axis is the position of the rotor in mechanical degrees and the vertical axis is the current in Amperes
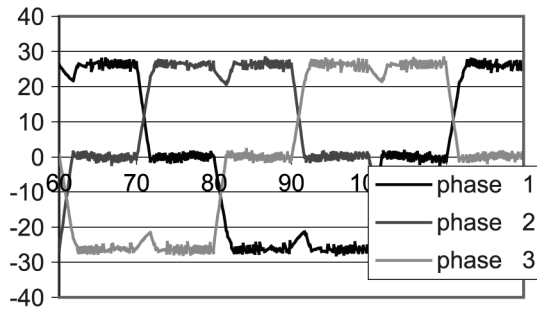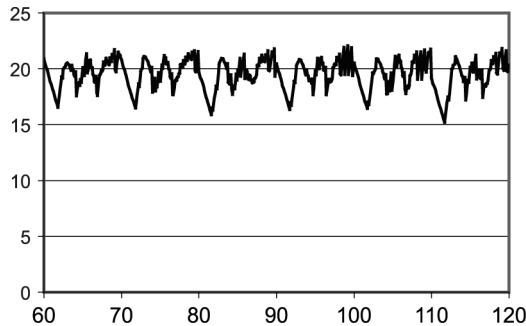

Figure 11.
Electromagnetic torque at full load. The horizontal axis is the position of the rotor in mechanical degrees and the vertical axis is the electromagnetic torque in Newton-meters

$d_{cr} = 7,850 \text{kg/m}^3$, $q_t = 2.5 \text{W/kg}$, $f_t = 50 \text{Hz}$, $B_t = 1.5 \text{T}$, $h = 10 \text{W/m}^2/\text{K}$, $T_{ext} = 50°C$, and $k_{foi} = 0.95$.

The structure is characterized by the following relation between the number of slots and the number of magnets: $N_e = (3/2)p$. The mechanical losses are estimated to $P_m = 15 \text{W}$. Finally, the leakage flux coefficient is identified by FEA: $k_{fui} = 0.8$.

2.2.10 Specifications. The specifications give the nominal torque as well as the rated speed: $C = 20 \text{N m}$ and $\Omega = 721\pi/30 \text{rad/s}$. The maximal speed reached at no-load is also specified $\Omega_{max} = 1442\pi/30 \text{rad/s}$.

2.3 Matrix of influences and design parameters

The choice of the design parameters is not unique. It is defined by the physical phenomena taken in consideration and reflects the designer's intentions. A necessary adequacy between the ranking of the sizing equations and the choice of the design parameters can be verified with the matrix of influences (Figure 12). Every line is associated to an equation and every column to a parameter. The coefficient a_{ij} of the matrix is one if the parameter x_j appears in the equation $g_i(x_1, \cdots, x_n)$ and zero otherwise. While classifying the parameters and the equations in the order of apparition, the matrix must be lower triangular so that the sizing can be made sequentially. Thus, every parameter deducts itself from those already calculated and of
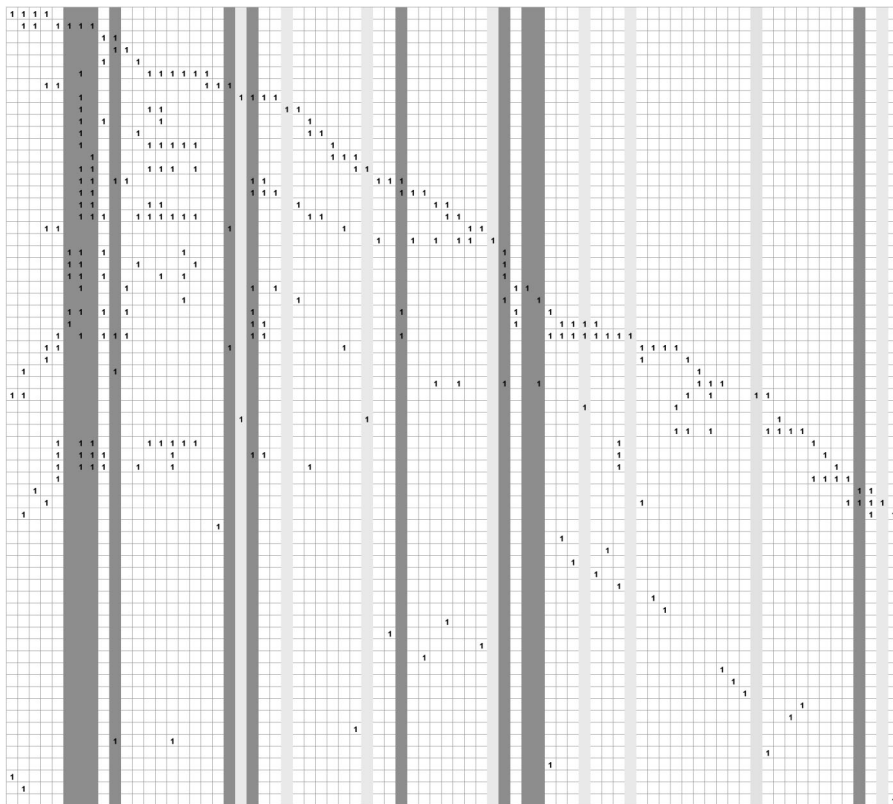

Figure 12.
Original matrix of
influences

an unique equation. On the contrary, a global resolution of the system of equations is necessary and requires particular numeric techniques because the equations are generally non-linear.

The initial matrix consists of 67 lines or equations and 78 columns or parameters. It is necessary to add 11 equations therefore so that the matrix is squared. These equations serve to fix the value of 11 input parameters arbitrarily. The choice of the authors concerns the following parameters: the bore diameter, the magnetic length, the ratio of the rotor length on the stator length, the thickness of air gap, the voltage of the DC bus, the magnetic inductions in the air gap, the teeth, the rotor yoke, the stator yoke, the current density and the number of pole-pairs. For the magnetic inductions and the current density, the minimal and maximal admissible values are known, do not vary with the size and weakly with the application of the machine and are directly interpretable by the electric machines manufacturers (Figure 12).

To get a lower triangular matrix, it is necessary to change the order of apparition of the parameters and equations, i.e. to permute the columns and lines. A specific algorithm can be found in Allain (2003). Starting from the left top of the matrix are first the specifications data, then the properties of the materials and finally, the input parameters. This part is diagonal. Then comes an orthogonal trapeze constituted by the sizing equations. In Figure 13, it appears that the final matrix is not quite triangle and that a sequential resolution is not possible. It is necessary to solve a system of 78 non-linear equations with 78 unknowns. In fact, only seven equations must be solved simultaneously, the other equations being solved sequentially. It must be noticed that use of equation (33) instead of equation (34) maintains the lower triangular structure of the matrix despite equation (33) being more complex.

Another approach is to choose an overestimated system that is a number of unknowns inferior to the number of equations. Then, there is infinity of solutions. It is however, possible to find a unique solution by formalizing a problem of optimisation like that described in the following section.

Two facts must be emphasized. First, the total number of conductors $(3/2)n$ must be approximate to the nearest multiple of two times the number of slots N_e. Secondly, the calculation of the slot height hd requires the solving of the second-order equation whose determinant can be negative for a low current density, for example. It is equal to zero when the slot has a triangular shape and the main tooth and the intermediate tooth touch themselves on the stator yoke side.

3. Results of the sizing

The input parameters have the following values: $D_s = 189\,\text{mm}$, $B_e = 0.75\,\text{T}$, $\delta = 3\,\text{A/mm}^2$, $B_d = 1.8\,\text{T}$, $B_{cs} = 0.8\,\text{T}$, $L_m = 45\,\text{mm}$, $r_{rs} = 1.11$, $e = 0.8\,\text{mm}$, $U_{DC} = 120\,\text{V}$, $B_{cr} = 1.2\,\text{T}$ and $p = 6$. The unknowns are then calculated from the data of the specifications, the material properties and the sizing equations: $\alpha = 30°$, $\beta = 30°$, $\alpha_i = 6°$, $k_v = 2$, $I = 25.168\,\text{A}$, $n = 249.162$, $li = 4.123\,\text{mm}$, $ld = 20.617\,\text{mm}$, $eb = 6.569\,\text{mm}$, $hcs = 23.194\,\text{mm}$, $Ba = 0.838\,\text{T}$, $hcr = 17.413\,\text{mm}$, $S_{enc} = 6,271\,\text{mm}^2$, $hd = 24.934\,\text{mm}$, $D_{int} = 79.607\,\text{mm}$, $f = 72.1\,\text{Hz}$, $hc = 3.467\,\text{mm}$, $hi = 3.591\,\text{mm}$, $R_{tb} = 17.294\,\text{mm}$, $L_{ds} = 101.7\,\text{mm}$, $L_{tot} = 95.929\,\text{mm}$, $M_{cs} = 2.646\,\text{kg}$, $M_{ds} = 2.862\,\text{kg}$, and $P_f = 21.096\,\text{W}$. This resolution is sequential.

The seven equations solved simultaneously give: $T_a = T_{cu} = 102.4°\text{C}$, $ha = 4.091\,\text{mm}$, $D_{ext} = 233.608\,\text{mm}$, $R_{ph} = 36\,\text{m}\Omega$, $P_j = 45.713\,\text{w}$, $S_{ext} = 0.156\,\text{m}^2$.
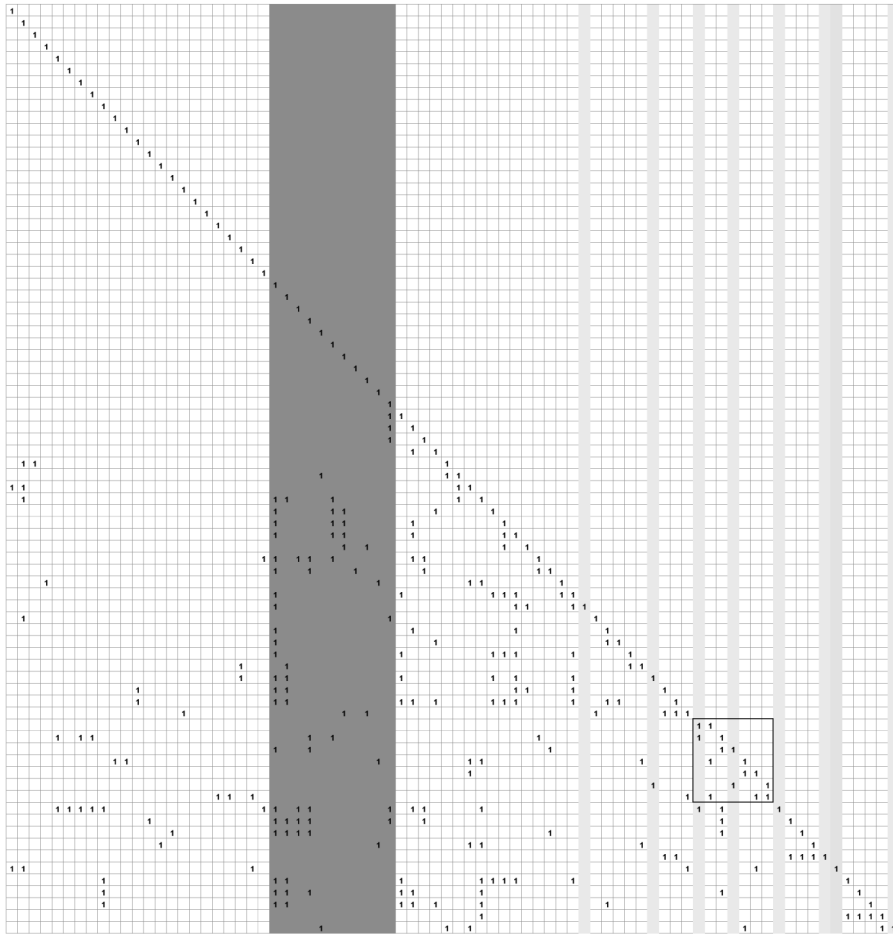
Figure 13.
Final matrix of influences.
The box shows the seven
equations that have to be
solved simultaneously

The continuation of the calculations is sequential: $I_{max} = 278.44$ A, $M_a = 0.925$ kg, $M_{cr} = 4.637$ kg, $M_{cu} = 2.854$ kg, $M_{tot} = 13.924$ kg, $\eta = 94.812$ per cent, $\psi_{enc}/I_{rc} = 4.351 \times 10^{-5}$ Wb/A, $\psi_{ent}/I_{rc} = 7.399 \times 10^{-4}$ Wb/A, $\psi_{bec}/I_{rc} = 7.83 \times 10^{-5}$ Wb/A, $L_{ph} = 1.353$ mH, and $t_1 = 0.572$ ms.

A prototype has been manufactured according to these parameters as shown in Plate 3. Measurements validate the sizing program.

4. Optimisation problems

The aim is to design a motor with the best efficiency η while meeting technical commitment. First, the total mass of the active parts M_{tot} must not exceed 15 kg. The outer diameter D_{ext} must be lower than 340 mm so that the motor fits into the rim of a wheel. The inner diameter D_{int} must be superior to 76 mm for mechanical reasons. The magnets must support a current in the phases I_{max} of 125 A (five times the rated

Plate 3.
Prototype of the wheel
motor. The inner stator is
visible with the coils rolled
up around the teeth
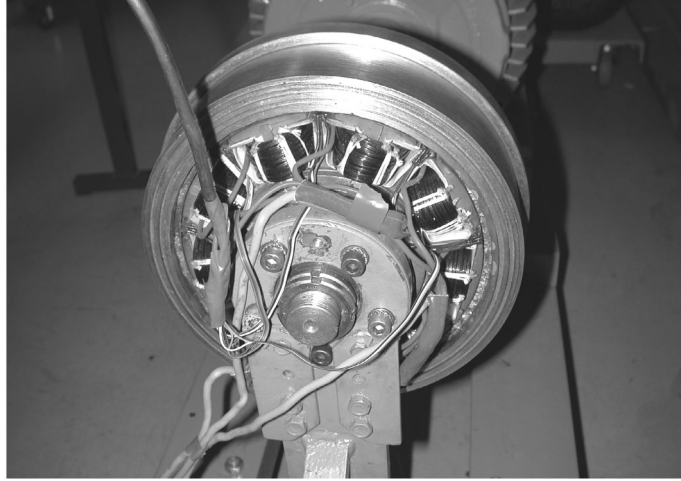
current) without demagnetisation. Finally, the rise time of the current t_1 must represent less than a tenth of the width of the plateau of EMF so that the current and the EMF stay in phase from the starting until the rated speed.

According to the number and the nature of the parameters considered, three specification sheets are proposed.

4.1 Five parameters problem

The values of five design variables (input parameters) are to be found: D_s, B_e, δ, B_d and B_{cs}. The six other input parameters are fixed: $L_m = 45$ mm, $r_{rs} = 1.11$, $e = 0.8$ mm, $U_{DC} = 120$ V, $B_{cr} = 1.2$ T and $p = 6$.

The design problem is then transformed as an optimisation problem:

$$
\begin{aligned}
\text{Maximise} \quad & \eta \\
\text{with} \quad & 150\,\text{mm} \leq D_s \leq 330\,\text{mm}, \quad 0.9\,\text{T} \leq B_d \leq 1.8\,\text{T} \\
& 2.0\,\text{A/mm}^2 \leq \delta \leq 5.0\,\text{A/mm}^2, \quad 0.5\,\text{T} \leq B_e \leq 0.76\,\text{T}, \\
& 0.6\,\text{T} \leq B_{cs} \leq 1.6\,\text{T} \\
\text{s.t.} \quad & M_{tot} \leq 15\,\text{kg}, \quad D_{ext} \leq 340\,\text{mm}, \quad D_{int} \geq 76\,\text{mm}, \\
& I_{max} \geq 125\,\text{A}, \quad \text{discr}(D_s, \delta, B_d, B_e) \geq 0, \quad T_a \leq 120°\text{C}
\end{aligned}
\tag{62}
$$

where η, M_{tot}, D_{ext}, D_{int}, I_{max}, and T_a are results of the sizing program and discr(D_s,δ,B_d,B_e) is the determinant used for the calculation of the slot height. This last constraint must absolutely be verified before the execution of the sizing program.

4.2 Ten parameters problem

In this formulation, only the number of pole-pairs is fixed: $p = 6$. Supplementary constraints are added on the total axial length $L_{tot} \leq 100$ mm, and the current rise time $t_1 \leq (1/30f)$. The intervals of variation of the new parameters are:

$$30\,\text{mm} \leq L_\text{m} \leq 90\,\text{mm}, \quad 0.8 \leq r_\text{rs} \leq 1.2, \quad 0.3\,\text{mm} \leq e \leq 2\,\text{mm}$$
$$0.6\,\text{T} \leq B_\text{cr} \leq 1.6\,\text{T} \quad \text{and} \quad 50\,\text{V} \leq U_\text{DC} \leq 200\,\text{V} \tag{63}$$

4.3 Eleven parameters problem
In this last formulation, the number of poles-pairs is the new integer parameter and only the even values are kept so that the winding is feasible:

$$p = 2k, \; k \in N^+ \quad \text{and} \quad N_\text{e} = \frac{3}{2}p = 3k \tag{64}$$

For all these formulations, the total number of conductors is rounded or not, according to the features of the optimisation method used.

5. Benchmark's special features
It is not necessary to present the optimisation methods neither to compare them. Nevertheless, one deterministic method is used and permits to highlight the special features of the benchmark.

The sequential quadratic programming (SQP) method is a non-linear programming method. It has been recognized as one of the most efficient methods for solving small and medium size constrained problems. Owing to a design environment (www.designprocessing.com), the analytical formulae of the model are derived exactly influencing then, in a very direct way, the performances of this approach.

Starting points $2^5 = 32$, one at each corner of the design space, are tested and lead to two very different local optimums (Table I). Thus, the problem is multimodal and a deterministic local optimisation method is not able to find the global optimum with certainty. As stochastic methods are known to be global but suffer from low accuracy and high computation time, this problem can be a very interesting benchmark for optimisation algorithms. Hybrid methods, i.e. combination of optimisation methods of different kind, and heuristics may lead perhaps to better results.

Number of points	24 (75 per cent)	8 (25 per cent)
B_cs (T)	0.8958	1.6
B_d (T)	1.8	1.211-1.292
B_e (T)	0.6481	0.6464-0.7215
δ (A/mm^2)	2.044	3.174-3.414
D_s (mm)	201.2	197.7-202.9
D_ext (mm)	238.9	240.8-241
D_int (mm)	76	76.02-76.55
I_max (A)	125	126.5-158.8
M_tot (kg)	15	15
η (per cent)	95.32	94.16-94.24
T_a (°C)	95.35	106.9-107.9
Iterations	13-119 (41)	61-137 (97)

Note: Notation: min-max (average)

Table I.
Optimisation results with
SQP method

6. Conclusion

In this paper, the optimal design of a brushless DC motor is proposed to become an analytical benchmark for the comparison of optimisation methods. This constraint optimisation problem is clearly multimodal as shown in the results of one deterministic method. As stochastic methods are known to be global but suffer from low accuracy and high computation time, hybrid methods and special heuristics may lead to better results.

References

Allain, L. (2003), "Capitalisation et traitement des modèles pour la conception en génie électrique", thèse de doctorat en génie électrique, INPG, Grenoble,.

Brisset, S., Gillon, F. and Brochet, P. (2000), "Numerical experimental designs applied to the modeling of brushless direct current motors", *ICEM*, pp. 1540-4, 28-30 August.

Brisset, S., Odoux, G. and Brochet, P. (2001), "Design of a brushless DC wheel motor for a solar vehicle", *ElectroMotion*, pp. 519-24.

Fitan, E., Messine, F. and Nogarède, B. (2004), "The electromagnetic actuator design problem: a general and rational approach", *IEEE TMAG*, Vol. 40 No. 3, pp. 1579-90.

Higuchi, T., Oyama, J. and Abe, T. (2002), "Design optimization of surface PM synchronous motor for servo usage", *ICEM*, No. 604, pp. 1-6.

Miller, T.J.E. and Hendershot, J.R. Jr (1994), *Design of Brushless Permanent-Magnet Motors*, Magna Physics Publishing and Clarendon Press, Oxford.

(S. Brisset is a graduate of Engineer School in 1992 at Ecole Centrale de Lille, France, PhD in Electrical Engineering in 1995 at Université des Sciences et Technologies de Lille. He joined Ecole des Hautes Etudes Industrielles in 1996 and Ecole Centrale de Lille in 2001 where he is now associate professor at Laboratoire d'Electrotechnique et d'Electronique de Puissance (L2EP). His main interests are the simulation, design and optimization of electric machines.

P. Brochet is a full time professor at Ecole Centrale de Lille (France) and a researcher in the Laboratory L2EP (Laboratoire d'Electrotechnique et d'Electronique de Puissance). His researches are on the design of electrical machines, particularly methodology, specific tools like optimization, design of experiments, numerical models. He is the manager of the team COME (Design and Optimization of Electrical Machines.))